ADVANCED MATERIALS
www.advmat.de

Nanoporous Gyroid Nickel from Block Copolymer Templates via Electroless Plating

Han-Yu Hsueh, Yen-Chun Huang, Rong-Ming Ho, Chih-Huang Lai, Taichi Makida, and Hirokazu Hasegawa*

Metallic nanoporous materials (MNMs) are 3D nanostructures composed of interconnected metallic particles or filaments that exhibit high porosity and large surface area. Combining the nature of metals and the unique material characters of nanostructures, MNMs have exceptional properties, including low relative density (ρ_{MNMs}/ρ_{bulk}), enhanced plasmonic behavior, high strength-to-weight ratio, and size-effect-enhanced catalytic behavior. These properties are of great interest in many fields of application including battery-like supercapacitors, high-power-density batteries, viable hydrogen storage, electromagnetic composites, surface-enhanced Raman spectroscopy, antimicrobial scaffolds, filtration and desalination, lightweight structures, heat sinks, ultrahigh field electromagnets, and magnetic media.[1] MNMs are much more difficult to fabricate in comparison with nanoporous materials of other substances. For bottom-up methods, only a few synthetic pathways have been demonstrated; for instance, aerogels with metallic backbones result from directly assembling metal nanoparticles into gels via sol-gel process. In contrast, using a top-down approach, nanoporous Au can be prepared via selective removal of Ag from a Au–Ag alloy (a process called dealloying). The feature size in nanoporous Au can be controlled over a wide range from 10 nm to the micrometers through a simple annealing procedure.[2] However, the majority of top-down methods suffer problems resulting from length-scale-dependent phenomena in scaling to the nanometer scale. Although different methods of preparing MNMs have been demonstrated, how to achieve the production of large-area continuous films or bulks with long-range order and precisely controlled pore geometries remains a challenge.

H.-Y. Hsueh, Prof. R.-M. Ho
Department of Chemical Engineering
National Tsing Hua University
Hsinchu 30013, Taiwan
E-mail: rmho@mx.nthu.edu.tw
Y.-C. Huang, Prof. C.-H. Lai
Department of Materials Science and Engineering
National Tsing Hua University
Hsinchu 30013, Taiwan
T. Makida, Prof. H. Hasegawa
Department of Polymer Chemistry
Graduate School of Engineering
Kyoto University
Nishikyo-ku, Kyoto, 615-8510, Japan

DOI: 10.1002/adma.201100883

A method to acquire well-defined MNMs has been developed by deposition of metals into templates with desired channels, such as mesoporous silica (MCM materials)[3] and arrays of colloidal crystals.[4,5] Although mesoporous silica with different framework structures and pore sizes has been successfully synthesized, this approach generally involves multistep process and it is hard to acquire the production of large-area continuous films. As for the exploitation of the arrays of colloidal crystals, their micrometer size is limited for the applications in nanotechnologies. In recent decades, block copolymers (BCPs) have been extensively investigated because of their ability to self-assemble into various ordered nanostructures, such as spheres, cylinders, gyroids, and lamellae.[6] Moreover, by taking advantage of the degradable character of BCPs, nanoporous polymer materials can be prepared by removal of the constituted components in BCPs through ozonolysis,[7] UV degradation,[8] and reactive ion etching.[9] Also, polylactide-containing BCPs (such as polystyrene-*b*-poly(D,L-lactide) (PS-PLA) and polystyrene-*b*-poly(L-lactide) (PS-PLLA)) can be used for the fabrication of nanoporous polymer materials from which polylactides can be hydrolytically degraded in base aqueous solution.[10,11]

Among all of the nanostructures resulting from BCP self-assembly, the gyroid is one of the most appealing morphologies for practical applications because of its unique texture with a matrix and two continuous networks in 3D space.[12–14] After the selective degeneration of the minor phase in the polymer matrix, the gyroid nanostructure could be exploited to create fully interconnected nanochannels. Because of the high porosity and large surface area, nanoporous polymer materials resulting from BCP gyroid are very promising for use in a variety of applications, such as catalysts,[15] ceramic membranes,[16–18] hybrid solar cells,[19] membrane reactors,[20–24] and low refractive index materials.[24] Also, nanoporous polymer materials can be used as templates for reactions. By exploiting a templating process (i.e., nanoreactor concept), reactions such as electrochemical deposition[19,21,23] and sol-gel processes[24] can be carried out within the BCP templates for the manufacturing of nanoporous inorganic materials with precisely controlled textures.

Nickel (Ni) materials, in particular with nanostructured textures, are very important catalytic materials and have been widely used in science and industry. A variety of approaches, such as electrochemical deposition,[25,26] hydrothermal synthesis,[27] spontaneous coalescence of nanoparticles,[28] and electroless plating,[15] have been well demonstrated for the manufacturing of anisotropic Ni nanoparticles and 1D Ni nanostructures. For instance, Hashimoto et al. used a polystyrene-*b*-polyisoprene BCP to prepare a PS template with ordered nanochannels through the ozonization of polyisoprene. Consequently, Ni

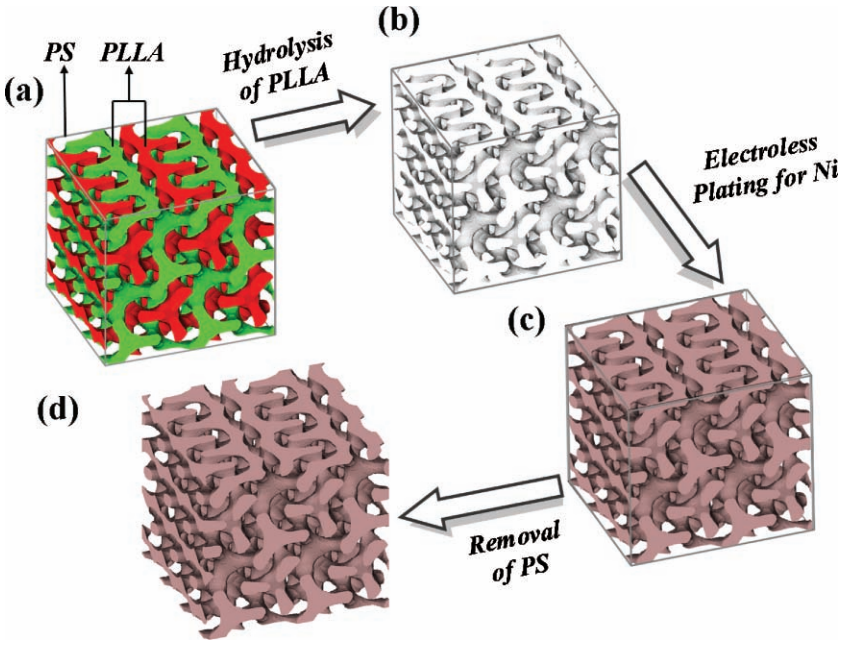

Figure 1. Schematic illustration for the creation of well-ordered nanoporous gyroid Ni from BCP templates. a) PS-PLLA gyroid phase showing the skeleton of the double gyroid structure with two identical networks (green and red). b) Gyroid-forming nanoporous PS template after removal of the minor PLLA network. c) PS/Ni gyroid nanohybrids via templated electroless plating. d) Nanoporous gyroid Ni after removal of the PS template by dissolution using THF.

nanoparticles (10 nm in diameter) were generated in the nanochannels via electroless plating.[15] Nielsch et al. deposited Ni into anodic aluminum oxide film via a pulsed electrochemical deposition to prepare monodisperse Ni nanowires.[25] Qian et al. demonstrated the fabrication of single-crystal Ni nanobelts (500–1000 nm in width) by using a complex-surfactant-assisted hydrothermal reduction method at a relatively low temperature (110 °C).[27] Additionally, Bittner et al. demonstrated that the central channels of the tobacco mosaic virus could be used as a template to synthesize nickel nanowires.[29] However, little work on the preparation of nanoporous Ni bulk has been reported to date.[30]

In this study, we demonstrate a new approach to create free-standing MNMs by using gyroid-forming nanoporous polymer as a template for electroless plating, followed by removal of the template. **Figure 1** illustrates the method. A PS-PLLA BCP with a molecular weight of 61 000 g mol^{-1} and a PLLA volume fraction of 39% was synthesized (see Supporting Information for details).[31] A double gyroid phase consisting of co-continuous PLLA networks in a PS matrix can be formed after solution casting of the synthesized PS-PLLA followed by quenching from a microphase-separated melt. After hydrolytic treatment, the PLLA networks can be selectively removed to give a PS matrix possessing interconnected air networks as a template for electroless plating. The formation of Ni from electroless plating is an autocatalytic reduction process in an aqueous Ni ion solution.[32] Subsequently, gyroid-forming nanohybrids with bicontinuous metallic networks can be fabricated. As a result, free-standing, nanoporous gyroid metals can be successfully fabricated after removal of the PS matrix by dissolution using tetrahydrofuran (THF). Unlike electrochemical deposition, the process of electroless plating (i.e., chemical deposition) is not necessary to pass an electric current through the solution to form a deposit; namely, there is no need for conductive substrates to create the monoliths of MNMs. Also, the method is very comprehensive because there are many available recipes for the deposition of various metals by using electroless plating. To the best of our knowledge, this is the first time well-defined, free-standing MNMs with high porosity and surface area have been obtained using such a straightforward method.

Figure 2a shows the transmission electron microscopy (TEM) image of the microsection of solution-cast PS-PLLA sample with specific thermal treatment as described. The PS matrix, selectively stained with RuO_4, appears dark whereas the PLLA microdomains appear bright. The [100] projected image of the PS-PLLA suggests the formation of a gyroid phase. Corresponding 1D small-angle X-ray scattering (1D SAXS) profiles (**Figure 3**a) further confirm the observed gyroid phase with a space group of *Ia3d* at which scattering peaks are found at the q^* ratios of $\sqrt{6}:\sqrt{8}:\sqrt{14}:\sqrt{16}:\sqrt{32}:\sqrt{50}$. $q^* = 4\lambda^{-1}\sin\theta$, where 2θ is the scattering angle. The interdomain spacing of $(211)_{gyroid}$ ($d_{(211)G}$) was determined to be approximately 40.9 nm from the primary reflection. After hydrolysis in a mild aqueous base, the PLLA blocks of the PS-PLLA could be removed completely (Figure S1, Supporting Information). Figure 3b displays the 1D SAXS profile of the PS-PLLA after hydrolysis; the diffraction peaks at the q^* ratios remain unchanged compared to Figure 3a, reflecting the

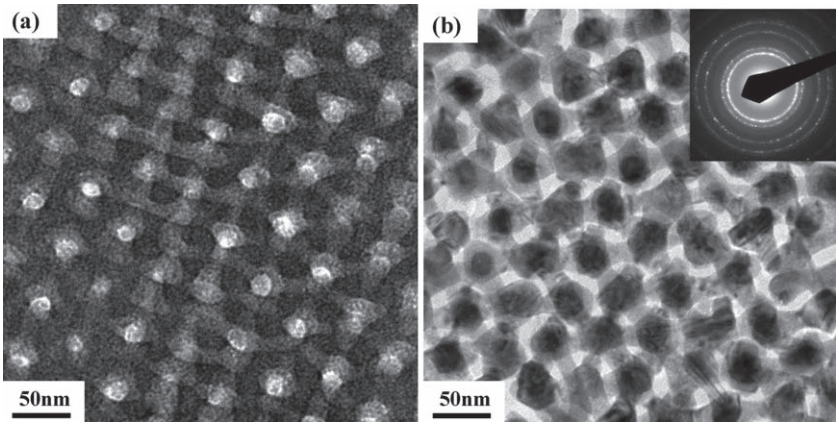

Figure 2. The [111] projected TEM microscopy images of a) PLLA gyroid phase in PS-PLLA with RuO_4 staining and b) PS/Ni gyroid nanohybrids without staining. The inset shows the selected area electron diffraction (SAED) pattern of Ni gyroid nanostructure in the nanohybrids.

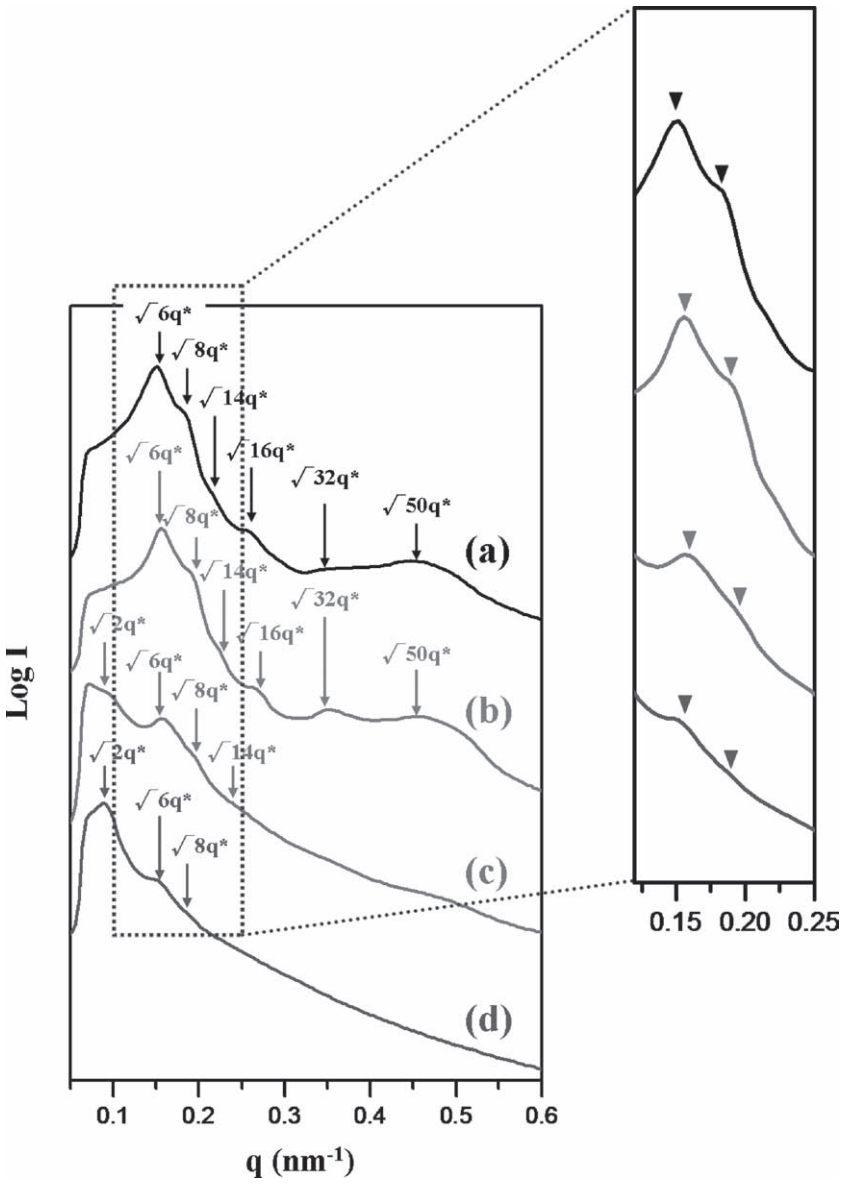

Figure 3. 1D SAXS profiles of a) PS-PLLA BCPs after quenching from microphase-separated, ordered melt, b) nanoporous PS template after removal of the PLLA blocks in PS-PLLA BCP by hydrolysis, c) PS/Ni gyroid nanohybrids, and d) nanoporous gyroid Ni from PS/Ni gyroid nanohybrids after removal of the PS template by dissolution using THF. The inset shows the enlarged area of q scale from 0.10 nm^{-1} to 0.25 nm^{-1}. The triangles in the inset mark the scattering peaks of √6 and √8 for the gyroid nanostructure.

successful templating. The interdomain spacing of $(211)_{gyroid}$ ($d_{(211)G}$) of the nanoporous PS template was determined to be approximately 39.8 nm from the primary reflection, indicating that there was a 2.6% shrinkage of its original size. We speculate that the change in the interdomain spacing is attributed to the cavitation effect resulting from removal of the residual solution of PLLA hydrolysis, leading to a reduction in proportional dimension of the gyroid feature. Consequently, a PS matrix with bicontinuous nanochannels was fabricated and employed as a template for the following electroless plating. The porosity and interfacial area per gram of the nanoporous PS template were approximately 37% and 97 $m^2 g^{-1}$ as determined by nitrogen adsorption experiments and Brunauer–Emmett–Teller analyzer (BET) analysis, respectively.

The properties of Ni prepared via electroless plating are dependent upon the contents of the Ni deposits. For example, if sodium hypophosphite is used as a reducing agent, a Ni–P alloy is usually found after electroless plating. As the phosphorus content increases, Ni deposits show decreasing catalytic efficiency and magnetization. To acquire pure Ni deposits, a modified Ni electroless plating was developed here. The nanoporous PS templates were soaked in an aqueous Pd^{+2} solution mixed with ethanol and HCl (1 N). Here, ethanol solvent was used to promote the wetting tendency of the activating solution into the PS templates through capillary force. HCl was used to enhance the solubility of Pd^{+2} in ethanol solvent. After washing gently with an ethanol/H_2O solution to remove redundant Pd^{+2} covering from sample surfaces, the pore-filled templates with the Pd^{+2} solution were then immersed into a freshly prepared Ni bath mixed with ethanol, ammonia, and hydrazinium hydroxide at room temperature. Hydrazinium hydroxide was used as a reducing agent. Consequently, the nucleation of Pd clusters would be initialized, at which Pd^{+2} ions can be reduced to Pd clusters by hydrazinium hydroxide. Note that the concentration of activating solution prepared here was quite low, and redundant Pd^{+2} covering on sample surface was washed out. As a result, only a small amount of Pd clusters could be generated within the PS templates. Accordingly, Ni^{+2} were reduced to Ni arising from the catalytic sites of the Pd clusters. By taking advantage of the self-catalytic behavior of electroless plating for an automatically continuous process of Ni formation, the reduced Ni may serve as the new nucleus for the following Ni reduction so that the Ni deposition process could continue until the nanochannels were fully filled (see Supporting Information for experimental details). Without any sensitization process, activation and electroless plating process can be carried out in one pot with this modified electroless plating. We speculate that the rate of Ni reduction works together with the self-ordering (i.e., crystallization) process of Ni so as to result in the formation of high crystallinity Ni (see below for corresponding characterization).

Figure 2b presents the [111] projected image of the PS/Ni gyroid nanohybrids without staining. The projected image in Figure 2b is similar to Figure 2a but the contrast is reversed, suggesting that the PLLA blocks should be completely removed after hydrolysis and the formation of Ni can be successfully synthesized in the nanoporous PS templates via the modified

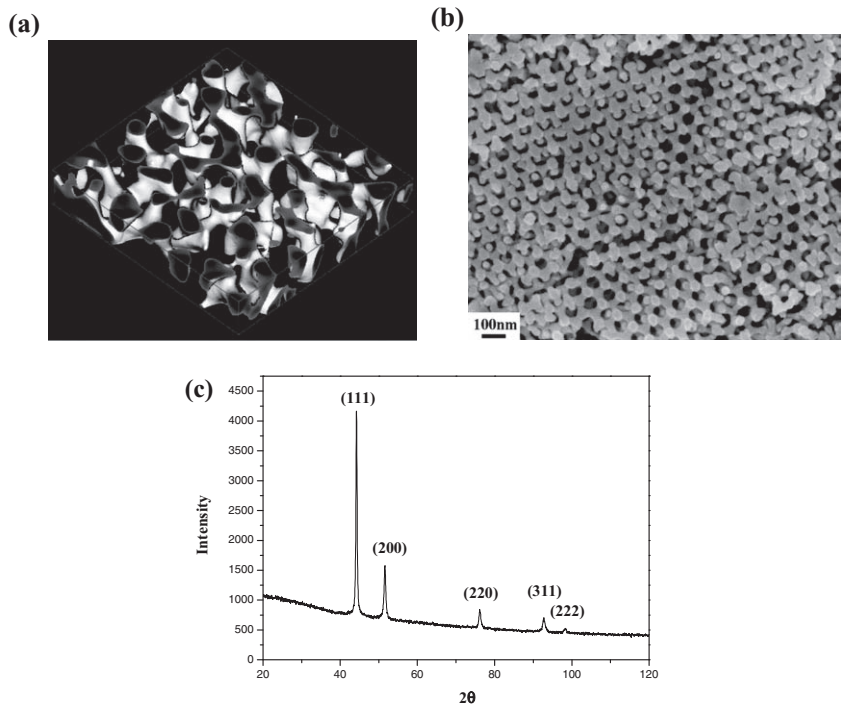

Figure 4. a) The reconstructed 3D image of well-ordered Ni double gyroid nanostructure in the PS/Ni gyroid nanohybrids. b) FESEM microscopy image of nanoporous gyroid Ni from the PS/Ni gyroid nanohybrids after removal of the PS templates. c) 1D XRD profiles of the nanoporous gyroid Ni.

electroless plating. Furthermore, a 3D image of the gyroid-forming Ni nanostructure in the PS matrix can be reconstructed from a set of 2D images at different tilt angles for projection (**Figure 4**a) (see Supporting Information for experimental details). As shown, a double gyroid Ni with bicontinuous networks in a PS matrix can be directly visualized. Figure 3c shows the 1D SAXS profile for the PS/Ni gyroid nanohybrids. On the basis of the characteristic first two reflections for the nanohybrids at a spacing ratio of √6 and √8, the gyroid-forming nanostructure of PS/Ni nanohybrids can be identified macroscopically. The interdomain spacing (39.8 nm ($d_{(211)G}$)) is the same as the nanoporous PS templates, indicating that the gyroid morphology can be retained after the templating process. Note that the q^* ratios of √2:√6:√8:√14 are different from the intrinsic PS-PLLA and the nanoporous PS template, and a new peak labeled with √2 might be attributed to the slight deformation of the gyroid nanostructure resulting in the formation of (110) reflection (that is a √2 peak),[33,34] as compared to the (211) and (220) reflections for √6 and √8 diffractions.

Figure 4b displays the field emission SEM (FESEM) microscopy image of the nanoporous gyroid Ni in the PS/Ni gyroid nanohybrids after removal of the PS templates. Low-magnification FESEM imaging of the nanoporous gyroid Ni was also conducted, and the results (Figure S3, Supporting Information) indicate that large-area continuous materials with precisely controlled pore geometries can be well prepared. Also, the inset of Figure S3 (Supporting Information) shows a photograph of the nanoporous gyroid Ni bulk, demonstrating the fabrication of a centimeter-sized crack-free sample. Fourier transform infrared (FT-IR) spectroscopy experiments (not shown) were conducted to further confirm that the PS can be completely removed. The structure of the nanoporous gyroid Ni can be further identified by SAXS (Figure 3d); the diffraction peaks are at the q^* ratios of √2:√6:√8. In contrast to the scattering results for the PS/Ni gyroid nanohybrids, the √2 peak can be clearly identified; previous studies suggested that the appearance of the √2 peak may be attributed to the formation of a pseudo-single gyroid nanostructure with a space group of $I4_132$.[24] Although the characteristic reflections for the samples containing Ni at high q range are relatively broad because of the effect from the form factor of Ni,[35] the identification of gyroid nanostructures could be verified by corresponding SAXS results consisting of the reflections at a q^* ratio of √6 and √8. The porosity of the nanoporous gyroid Ni was about 62% from nitrogen adsorption experiments, and the interfacial area per gram of the nanoporous gyroid Ni was calculated as 1467 m^2 mol^{-1} (25 m^2 g^{-1}). The intrinsic density of pure Ni without pores via the modified electroless plating was ≈8.0 g cm^{-3}. As a result, the density of nanoporous gyroid Ni was ≈3.05 g cm^{-3} (38% relative density).

To examine crystalline character of the nanoporous gyroid Ni, selected area electron diffraction (SAED) and X-ray diffraction (XRD) experiments were conducted. Inset of Figure 2b displays the SAED pattern of the Ni gyroid nanostructure in the nanohybrids taken from Figure 2b, and the diffraction rings can be indexed with the face-centered cubic (fcc) Ni polycrystals (Figure S4, Supporting Information). In addition to the reflections from the high crystallinity Ni, the reflections resulting from the NiO crystallites marked can be identified. We thus speculate that the NiO is generated from the oxidation of Ni exposed to air and moisture. The XRD results of the nanoporous gyroid Ni (Figure 4c) agree with the SAED results. All the diffractions can be indexed as fcc Ni with the lattice constant a = 3.540 Å, JCPDS card no. 4-856, corresponding to (111), (200), (220), (311), and (222), respectively. No characteristic peaks of impurities, such as NiO and $Ni(OH)_2$, could be detected. Both the SAED and XRD results demonstrate that well-defined crystalline character of Ni phase could be obtained under ambient conditions. Furthermore, X-ray photoemission spectroscopy (XPS) was used to examine the elemental composition of the nanoporous gyroid Ni (Figure S5, Supporting Information). Since no XPS peaks indicative of NiO species could be identified, it could be concluded that no significant amount of NiO species was present within the nanoporous gyroid Ni after the modified electroless plating. Note that the metallic materials with fine grains exhibit better mechanical strength and catalytic efficiency than the amorphous ones so as to be widely used in applications. Also, the results from energy dispersive X-ray spectroscopy (EDX) reflect that the amount of Pd atoms is insignificant, indicating the formation of high-purity crystalline Ni via the modified electroless plating (Figure S6, Supporting

Information). The magnetic property of nanoporous gyroid Ni was demonstrated (Supporting Information). In contrast to the magnetic properties of 3D ferromagnetic micrometer-size structures reported, such as Ni inverse opals,[36] the enhancement in the coercivity of PS/Ni gyroid nanohybrids examined here is remarkable and presumably attributed to the effect of nanoscale dimension (Figure S7, Supporting Information).

In conclusion, MNMs with well-ordered gyroid nanostructures were fabricated by using nanoporous polymer with gyroid nanochannels as a template for a modified electroless plating. The nanoporous polymer templates were obtained from the self-assembly of degradable block copolymer, PS-PLLA, followed by the hydrolysis of PLLA blocks. Templated electroless plating can be conducted under ambient conditions to create a well-ordered Ni gyroid nanostructure with high crystallinity in a PS matrix. After removal of the PS matrix, free-standing, nanoporous gyroid Ni can be successfully fabricated to give precisely controlled MNMs with high porosity and surface area. Those MNMs with the nature of porous metals and the unique material characteristics of well-ordered nanostructures would exhibit interesting photonic properties for novel applications including enhanced plasmonic behavior, photonic crystals, and metamaterials. This new approach for hybridization provides a precisely controlled method to fabricate nanohybrids and MNMs.

Experimental Section

The PS-PLLA BCP was prepared by a double-headed polymerization sequence. The PS-PLLA (molecular weight, $M_{n,PS} = 34\,000$ g mol^{-1}, $M_{n,PLLA} = 27\,000$ g mol^{-1}, polydispersity index, PDI = 1.21, $f_{PLLA}^{\nu} \approx 0.37 - 0.40$, where f_{PLLA}^{ν} is the volume fraction of PLLA) was prepared by solution casting from dichloromethane (CH_2Cl_2) solution (10 wt% of PS-PLLA) at room temperature. After quenching from microphase-separated ordered melt, the PLLA blocks of the PS-PLLA bulk samples were removed by hydrolysis. The nanoporous PS templates were soaked in an activating solution mixed with ethanol (45 mL), HCl (1 N, 5 mL), and $PdCl_2$ (0.05 g) with stirring at room temperature for several hours (3–4 h). Consequently, the pore-filled samples were immersed into a freshly prepared Ni bath at room temperature. In a Ni bath, 0.2 g of nickel chloride ($NiCl_2{\cdot}6H_2O$) was dissolved in a solution consisting of distilled water (20 mL), ethanol (5 mL), hydrazinium hydroxide (85%, 2 mL), and ammonia (2 mL). To create the nanoporous gyroid Ni, the nanoporous PS template of the PS/Ni gyroid nanohybrids was removed by washing with THF.

Supporting Information

Supporting Information is available from the Wiley Online Library or from the author.

Acknowledgements

The authors would like to thank the National Science Council of the Republic of China, Taiwan, for financially supporting this research under Contract No. Grant NSC NSC 99-2120-M-007 -003-. Ms. I -H. Wu of the Department of Applied Chemistry at NCTU is appreciated for her assistance with the FESEM experiments, as well the National Synchrotron Radiation Research Center (NSRRC) for its assistance in the Synchrotron SAXS experiments.

Received: March 8, 2011
Revised: April 18, 2011
Published online: May 20, 2011

[1] a) B. C. Tappan, S. A. Steiner, E. P. Luther, *Agnew. Chem. Int. Ed.* **2010**, *49*, 4544; b) D. R. Rolison, J. W. Long, J. C. Lytle, A. E. Fischer, C. P. Rhodes, T. M. McEvoy, M. E. Bourg, A. M. Lubers, *Chem. Soc. Rev.* **2009**, *38*, 226; c) B. Kang, G. Ceder, *Nature* **2009**, *458*, 190; d) M. C. Dixon, T. A. Daniel, M. Hieda, D. M. Smilgies, M. H. W. Chan, D. L. Allara, *Langmuir* **2007**, *23*, 2414; e) J. Biener, G. W. Nyce, A. M. Hodge, M. M. Biener, A. V. Hamza, S. A. Maier, *Adv. Mater.* **2008**, *20*, 1211; f) M. Nishizawa, V. P. Menon, C. R. Martin, *Science* **1995**, *268*, 700.

[2] a) J. Erlebacher, M. J. Aziz, A. Karma, N. Dimitrov, K. Sleradzki, *Nature* **2001**, *410*, 450; b) A. Wittstock, B. Neumann, A. Schaefer, K. Dumbuya, C. Kuebel, M. M. Biener, V. Zielasek, H.-P. Steinrueck, J. M. Gottfried, J. Biener, A. Hamza, M. Baeumer, *J. Phys. Chem. C* **2009**, *113*, 5593; c) J. Weissmüller, R. C. Newman, H.-J. Jin, A. M. Hodge, J. W. Kysar, *MRS Bull.* **2009**, *34*, 577.

[3] A. Monnier, F. Schuth, Q. Huo, D. Kumar, D. Margolese, R. S. Maxwell, G. D. Stucky, M. Krishnamurty, P. Petroff, A. Firouzi, M. Janicke, B. F. Chmelka, *Science* **1993**, *261*, 1299.

[4] A. A. Zakhidov, R. H. Baughman, Z. Iqbal, C. X. Cui, I. Khayrullin, S. O. Dantas, I. Marti, V. G. Ralchenko, *Science* **1998**, *282*, 897.

[5] P. Jiang, J. Cizeron, J. F. Bertone, V. L. Colvin, *J. Am. Chem. Soc.* **1999**, *121*, 7957.

[6] a) F. S. Bates, G. H. Fredrickson, *Annu. Rev. Phys. Chem.* **1990**, *41*, 525; b) F. S. Bates, G. H. Fredrickson, *Phys. Today* **1999**, *52*, 32.

[7] M. Park, C. Harrison, P. M. Chaikin, R. A. Register, D. H. Adamson, *Science* **1997**, *276*, 1401.

[8] T. Thurn-Albrecht, R. Steiner, J. DeRouchey, C. M. Stafford, E. Huang, M. Bal, M. Tuominen, C. J. Hawker, T. P. Russell, *Adv. Mater.* **2000**, *12*, 787.

[9] J. Y. Cheng, C. A. Ross, V. Z. H. Chan, E. L. Thomas, R. G. H. Lammertink, G. J. Vancso, *Adv. Mater.* **2001**, *13*, 1174.

[10] A. S. Zalusky, R. Olayo-Valles, C. J. Taylor, M. A. Hillmyer, *J. Am. Chem. Soc.* **2001**, *123*, 1519.

[11] a) W. H. Tseng, C. K. Chen, Y. W. Chiang, R. M. Ho, S. Akasaka, H. Hasegawa, *J. Am. Chem. Soc.* **2009**, *131*, 1356; b) Y. T. Tseng, W. H. Tseng, C. H. Lin, R. M. Ho, *Adv. Mater.* **2007**, *19*, 3584.

[12] D. A. Hajduk, P. E. Harper, S. M. Gruner, C. C. Honeker, G. Kim, E. L. Thomas, L. J. Fetters, *Macromolecules* **1994**, *27*, 4063.

[13] M. F. Schulz, F. S. Bates, K. Almdal, K. Mortensen, *Phys. Rev. Lett.* **1994**, *73*, 86.

[14] M. W. Matsen, M. Schick, *Phys. Rev. Lett.* **1994**, *72*, 2660.

[15] T. Hashimoto, K. Tsutsumi, Y. Funaki, *Langmuir* **1997**, *13*, 6869.

[16] V. Z.-H. Chan, J. Hoffman, V. Y. Lee, H. Latrou, A. Avgeropoulos, N. Hadjichristidis, R. D. Miller, E. L. Thomas, *Science* **1999**, *286*, 1716.

[17] A. C. Finnefrock, R. Ulrich, G. E. S. Toombes, S. M. Gruner, U. Wiesner, *J. Am. Chem. Soc.* **2003**, *125*, 13084.

[18] A. Jain, G. E. S. Toombes, L. M. Hall, S. Mahajan, C. B. W. Garcia, W. Probst, S. M. Gruner, U. Wiesner, *Angew. Chem. Int. Ed.* **2005**, *44*, 1226.

[19] E. J. W. Crossland, M. Kamperman, M. Nedelcu, C. Ducati, U. Wiesner, D. M. Smilgies, G. E. S. Toombes, M. A. Hillmyer, S. Ludwigs, U. Steiner, H. J. Snaith, *Nano Lett.* **2009**, *9*, 2807.

[20] M. Adachi, A. Okumura, E. Sivaniah, T. Hashimoto, *Macromolecules* **2006**, *39*, 7352.

[21] V. N. Urade, T. C. Wei, M. P. Tate, J. D. Kowalski, H. W. Hillhouse, *Chem. Mater.* **2007**, *19*, 768.

[22] A. S. Finnemore, M. R. J. Scherer, R. Langford, S. Mahajan, S. Ludwigs, F. C. Meldrum, U. Steiner, *Adv. Mater.* **2009**, *21*, 3928.

[23] S. Ndoni, L. Li, L. Schulte, P. P. Szewezykowski, T. W. Hansen, F. X. Guo, R. H. Berg, M. E. Vigild, *Macromolecules* **2009**, *42*, 3877.

[24] H. Y. Hsueh, H. Y. Chen, M. S. She, C. K. Chen, R. M. Ho, S. Gwo, H. Hasegawa, E. L. Thomas, *Nano Lett.* **2010**, *10*, 4994.

[25] K. Nielsch, F. Müller, A.-P. Li, U. Gösele, *Adv. Mater.* **2000**, *12*, 582.

[26] S. Z. Chu, K. Wada, S. Inoue, S. I. Todoroki, *Chem. Mater.* **2002**, *14*, 4595.
[27] Z. Liu, S. Li, Y. Yang, S. Peng, Z. Hu, Y. Qian, *Adv. Mater.* **2003**, *15*, 1946.
[28] T. Sehayek, M. Lahav, R. Popovitz-Biro, A. Vaskevich, I. Rubinstein, *Chem. Mater.* **2005**, *17*, 3743.
[29] M. Knez, A. M. Bittner, F. Boes, C. Wege, H. Jeske, E. Maiß, K. Kern, *Nano Lett.* **2003**, *3*, 1079.
[30] L. Sun, C. L. Chien, P. C. Searson, *Chem. Mater.* **2004**, *16*, 3125.
[31] R.-M. Ho, Y.-W. Chiang, C.-K. Chen, H.-W. Wang, H. Hasegawa, S. Akasaka, E. L. Thomas, C. Burger, B. S. Hsiao, *J. Am. Chem. Soc.* **2009**, *131*, 18533.
[32] G. O. Mallory, J. B. Hajdu, *Electroless Plating: Fundamentals and Applications*, American Electroplaters and Surface Finishers Society, Orlando, FL **1990**.
[33] B. J. Dair, C. C. Honeker, D. B. Alward, A. Avgeropoulos, N. Hadjichristidis, L. J. Fetters, M. Capel, E. L. Thomas, *Macromolecules* **1999**, *32*, 8145.
[34] S. Sakurai, D. Isobe, S. Okamoto, T. Yao, S. Nomura, *Phys. Rev. E* **2001**, *63*, 061803.
[35] a) Y. N. C. Chan, G. S. W. Craig, R. R. Schrock, R. E. Cohen, *Chem. Mater.* **1992**, *4*, 885; b) N. Sakamoto, M. Harada, T. Hashimoto, *Macromolecules* **2006**, *39*, 1116.
[36] T. S. Eagleton, P. C. Searson, *Chem. Mater.* **2004**, *16*, 5027.